Magnetization and electron paramagnetic resonance of Co clusters embedded in Ag nanoparticles

Magnetization and electron paramagnetic resonance of Co clusters embedded in Ag nanoparticles

R D Sánchez†§, M A López-Quintela†, J Rivas†, A González-Penedo†, A J García-Bastida†, C A Ramos‡, R D Zysler‡§ and S Ribeiro Guevara‡

† Departamentos de Física Aplicada y Química Física, Universidad de Santiago de Compostela, E-15076 Santiago de Compostela, Spain
‡ Centro Atómico Bariloche and Instituto Balseiro, (8400) San Carlos de Bariloche, Río Negro, Argentina

Abstract. We report magnetization and electron paramagnetic resonance (EPR) measurements on Co clusters embedded in Ag obtained by an inverse micellar technique. The cluster size ($\sim$10 atoms), the saturation magnetization (M_s), and the anisotropy constant were obtained from magnetization measurements at low temperature. In the as-prepared sample we found that $M_s/M_s^{\text{bulk}} = 0.44\pm0.05$. Reduction of the sample under a H_2 flux at 373 K leads to an enhancement of the ratio M_s/M_s^{bulk} to 1.16 ± 0.19—consistent with Co-cluster-beam experiments—and to an anisotropy constant of $K = (8.5 \pm 6.5) \times 10^7$ erg cm^{-3}, much larger than the corresponding bulk value. The EPR clearly shows the effect of dynamic narrowing due to superparamagnetic relaxation. Modelling the EPR spectra, we obtained independently the anisotropy energy value and the volume dispersion.

1. Introduction

Ultrafine magnetic particles play an important role in the fabrication of artificially structured materials. Granular magnetic solids are a good example of artificially structured materials and they are usually in the form of small ferromagnetic (FM) particles embedded in an immiscible matrix which may be insulating or metallic [1]. Actually, for many granular metals, Fe/Au, Fe/Cu, Co/Ag, Co/Cu, ..., it is possible to obtain FM particles in the nanometric range [1].

Achieving an understanding of the changing magnetic properties of small clusters and fine particles of transition metal ions is a challenge that has recently led to a considerable amount of work, both theoretical [2, 3] and experimental [4, 5]. In the last few years a great effort has been made to study the magnetic moment of free clusters by means of Stern–Gerlach experiments [5]. These experiments have clearly shown an enhancement of the magnetic moment as the size of the cluster decreases below $\approx$500 atoms.

In supported fine-particle systems, the sizes obtained range from a few nanometres to $\sim$1 μm and generally have a certain dispersion that depends on the preparation method. Recently, microemulsion techniques have yielded nanometric particles with small size dispersion [6–9]. Chen *et al* [8] report magnetic results for Co particles in microemulsions. These authors postulate that their particles with diameters in the range 18–45 Å are constituted by two magnetic components. One of these is FM with a magnetic moment comparable

§ Present address: Centro Atómico Bariloche, (8400) San Carlos de Bariloche, Río Negro, Argentina.

5643

to the bulk one and a second component characterized by an effective magnetic moment $\mu_s = 7.5 \pm 1\,\mu_B$ which they attribute to a 'shell' phase. Yet the origin of the magnetic moment of this shell phase is not clear and, as observed by the authors, the enhancement found for the magnetic moment turns out to be larger than the one observed in cluster-beam experiments [5]. More recently, Respaud *et al* report magnetization [10] and high-frequency ferromagnetic resonance [11] measurements on Co nanoparticles. These authors find an enhancement of the Co magnetic moment in agreement with the cluster-beam experiments [5] and effective magnetic anisotropies larger than for the bulk.

There is controversy regarding the effect of Ag covering of Co nanoparticles. On one hand Ag is a good candidate for preventing oxidation, but the effect on the magnetic properties of the Co nanoparticles has been claimed to produce important changes in the magnetic properties such as the coercive field [12], and to either change drastically the saturation magnetization [13] or not [14], and recent tight-binding calculations indicate that M_s is enhanced from the bulk value for small Co cluster size and also, for a given number of Co atoms, M_s depends on the size and shape of the Ag covering [15].

In this paper we present magnetization and EPR results for Co clusters embedded in Ag particles fabricated by microemulsion techniques. The Co nanoparticles were obtained by a technique similar to one described earlier [16] and coated '*in situ*' with Ag. The proportion of Co/Ag/organic components was determined by atomic emission spectroscopy and subsequently by neutron activation analysis. The measurements on the as-prepared samples were made in a superconducting quantum interference device (SQUID) magnetometer and they were characterized by means of EPR. The magnetization data were fitted to the exact result for a system of non-interacting particles in the presence of uniaxial anisotropy. For the as-prepared sample, the EPR was measured as a function of T ($300 \leqslant T$ (K) $\leqslant 535$) and interpreted within a model for superparamagnetic resonance. Thermal annealing at 373 K in a reducing H_2 atmosphere produces significant changes in the magnetization and EPR data, which were interpreted within the same models as were used for the as-prepared sample.

2. Experimental procedure

The microemulsions employed in the production of the particles were composed of *n*-heptane, aqueous solution, and aerosol-OT (AOT, sodium dodecylsulphosuccinate). The droplet size of these microemulsions was controlled by the ratio $R = [H_2O]/[AOT]$. This ratio was set at 10. The whole process for obtaining the particles was carried out in an inert glove box. For the formation of the magnetic cores two different microemulsions were prepared. The first one consisted of an aqueous solution of $Co(NO_3)_2 \cdot 6H_2O$ and the second one contained $NaBH_4$. The two microemulsions were mixed and the Co magnetic particles were formed inside the nanodroplets. Solid $NaBH_4$ was added in excess and then an aqueous solution containing $AgNO_3$ with a previously established molar ratio (Co/Ag $= 1/10$) were poured over this microemulsion containing the magnetic cores. The Ag^+ ions can only be reduced within the nanodroplets containing the Co particles. This process prevents surfactant from being present at the Co/Ag interface. The coated microparticles were separated from the solution by ultracentrifugation, washed several times with *n*-heptane and ethanol in order to remove AOT surfactant, and finally dried with acetone.

The samples were characterized by atomic emission spectroscopy, and found to have the composition Co 2.5%, Ag 39.1%, organic components 58.4% by weight. Independent neutron activation analysis was carried out to determine the total Co content, yielding the following values for the as-prepared sample: $2.36 \pm 0.06\%$ Co and $40.2 \pm 1.7\%$ Ag. Transmission electron microscopy and x-ray characterization for similarly prepared samples have been published

before [16]. We performed a heat treatment of part of the sample in a flowing H_2 atmosphere at 373 K for two hours. We will present the results for both as-prepared (AP) and heat-treated (HT) samples.

3. Results

3.1. Magnetization measurements

The magnetization data were obtained in a commercial Quantum Design SQUID magnetometer in the $2 < T$ (K) < 300 temperature range. In order to obtain the saturation moment of the particles it is necessary to measure the magnetization as a function of H at low temperatures. We assumed a density of 8.8 g cm^{-3}, corresponding to bulk Co. In figure 1 and figure 2 we have plotted M versus H/T for several values of T for the AP and HT samples respectively. It is observed that the experimental data do not collapse with H/T as would be expected for a classical Langevin function [17].
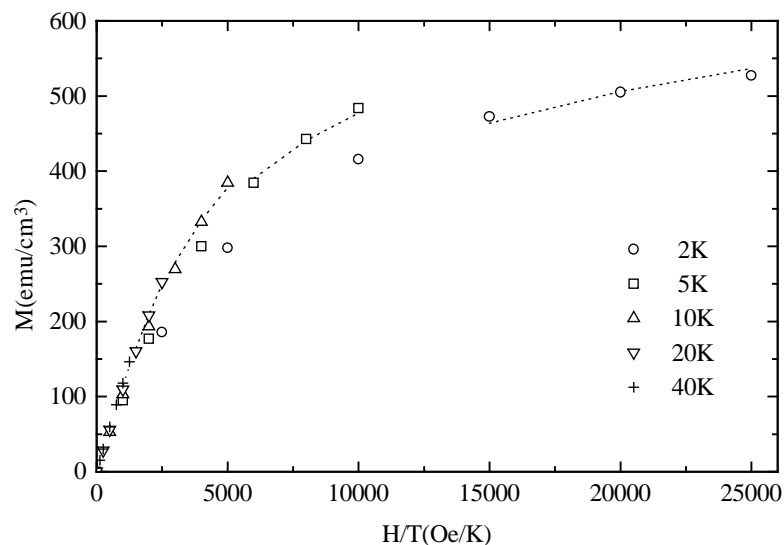

Figure 1. Magnetization of the as-prepared sample. A scaled plot of M versus H/T; the dotted curves are a simultaneous fit of all of the data with $H \geqslant 30$ kOe to a modified Langevin function given by equation (4.4) including the effect of a uniaxial anisotropy, and volume dispersion following a log–normal distribution.

In figure 3 we show zero-field-cooled (ZFC) and field-cooled (FC) magnetization measurements obtained under an applied field of $H = 50$ Oe for the AP and HT samples. The AP sample remains in a superparamagnetic [17] regime down to the lowest measured temperature (2 K) and shows no maximum as is commonly observed for larger particles [8, 9]. The HT sample shows a very large increase of the low-field magnetization when compared with the AP sample, and a maximum in M(ZFC) versus T at $T_m = 6.0$ K, associated with the blocking [18] of the superparamagnetic state. In the inset we show the inverse of the susceptibility. The magnetization above 50 K can be described by a Curie–Weiss law:
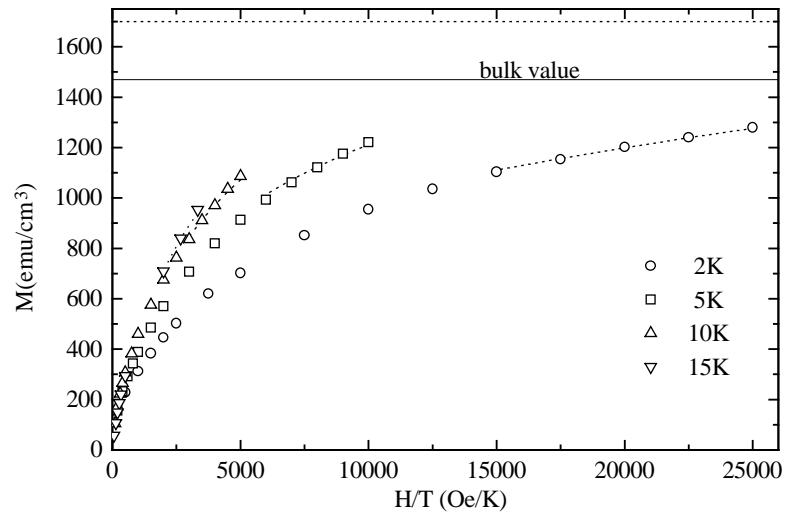
$$M/H = C/(T - \theta) \tag{3.1}$$

Figure 2. As figure 1, but for the heat-treated sample. The dotted horizontal curve corresponds to the best-fitted saturation magnetization.
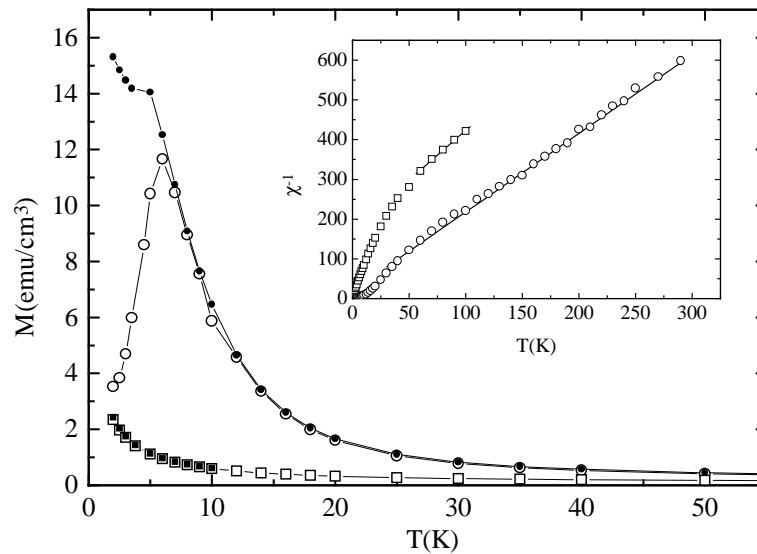

Figure 3. The magnetization temperature dependence at $H = 50$ Oe for as-prepared ($\square$) and heat-treated ($\bigcirc$) Co/Ag 1:10 samples. Open (full) symbols correspond to zero-field-cooled (field-cooled) magnetization measurements. The inverse susceptibility (inset) shows a Curie–Weiss-type behaviour showing antiferromagnetic interactions.

where θ is the Curie–Weiss temperature. A high-T fit of the inverse susceptibility

$$\chi^{-1}(T) = H/M(T)$$

to this functional form (full curves in the inset of figure 3) yields $\theta = -70 \pm 5$ K and $\theta = -10 \pm 6$ K for the AP and HT samples respectively, which indicates that antiferromagnetic

(AF) interactions are present in the AP sample, and that the magnitude of this interaction decreases significantly in the HT sample.

3.2. EPR measurements

EPR measurements were performed with an X-band Bruker SP-300 spectrometer operating at 9.44 GHz with a variable temperature cryostat. The AP sample was encapsulated in a quartz tube, and purged several times with Ar before sealing the tube. The EPR was recorded as a function of increasing T, for $T \geqslant 300$ K (figure 4). The circles correspond to a fit of the spectra to a model that includes uniaxial anisotropy and will be described below. It is observed that the most intense line narrows on increasing T and shifts slightly towards higher resonance fields. This is characteristic of the EPR of superparamagnetic particles [19–21]. At $T = 500$ K the spectrum can be characterized by a gyromagnetic factor $g = 2.12 \pm 0.03$, close to the reported g-value for films [22] ($g = 2.14 \pm 0.04$).
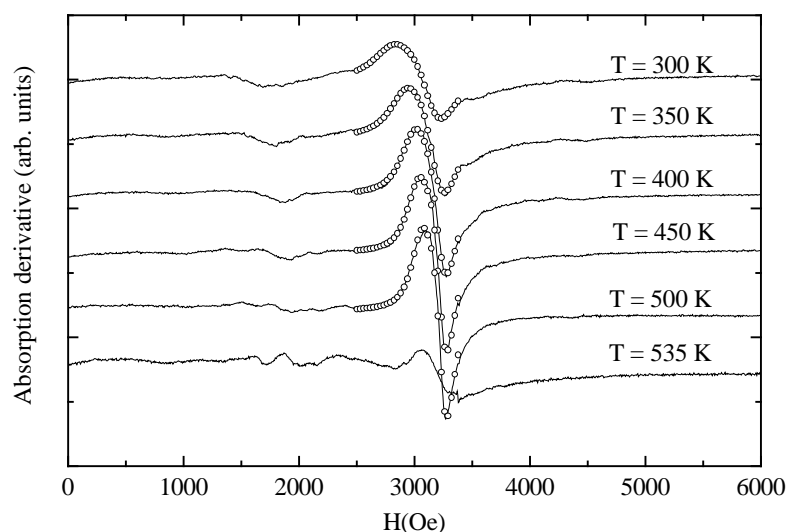

Figure 4. The X-band EPR absorption derivative for the AP sample taken at different temperatures. The circles correspond to a fit of the data to the model described in the text.

The EPR spectra obtained at $T > 500$ K are very different from the other spectra obtained at $T \leqslant 500$ K. Also, the room temperature EPR spectrum was not recovered after heating above 500 K, indicating an irreversible transformation. This result indicates a sample transformation, which was also previously observed from magnetization measurements on similar samples [16].

In figure 4 all of the EPR scans show an absorption near $H = 1500$–1700 Oe. This absorption shifts slightly to higher fields as T is increased and it splits into several lines above 450 K. For the H_2-reduced sample (HT) this low-field line disappears, but a broad line reappears if the sample is left in air for a period of one month (see figure 5). We therefore conclude that this low-field line may be associated with an oxide phase.

EPR spectra of the HT sample below room temperature are shown in figure 6. The circles correspond to a fit of the spectra to a model that will be described below.
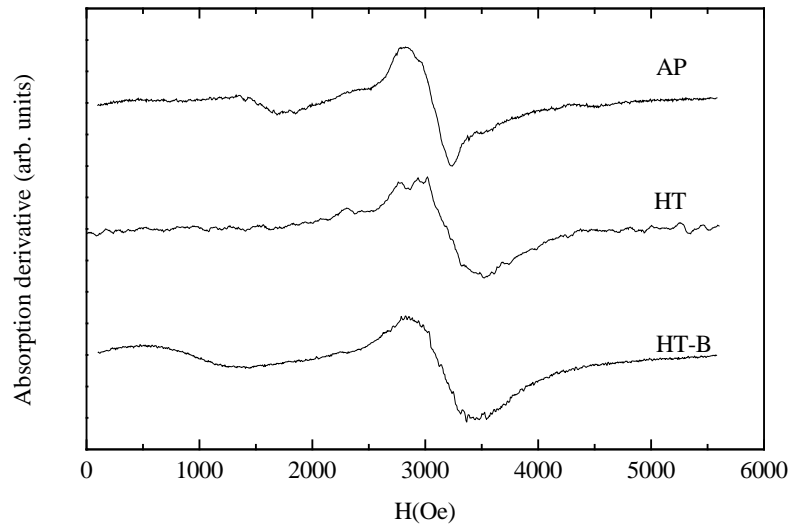
Figure 5. EPR absorption spectra of as-prepared (AP) and heat-treated (HT) samples, and samples heat treated after a month's exposure to air (HT-B). All spectra were taken at room temperature.
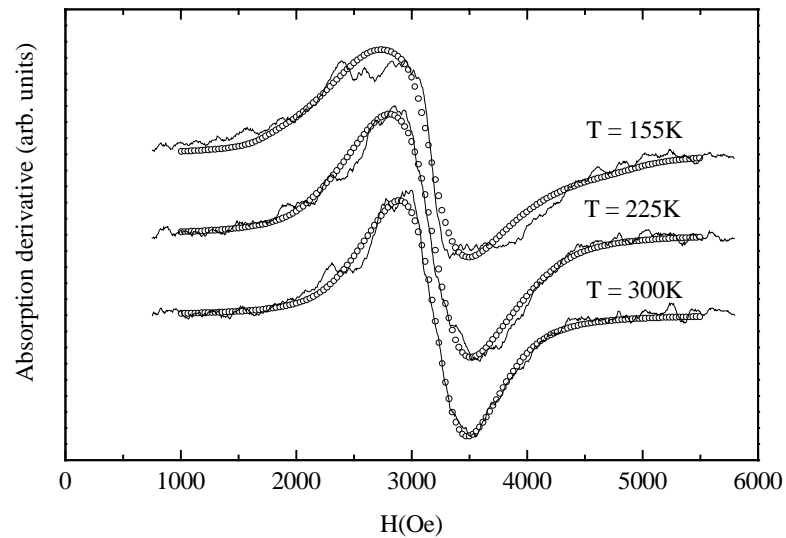
Figure 6. Low-temperature evolution of the HT EPR spectra. The dotted curves are fits using the same anisotropy, average volume, and dispersion for the three temperatures. The observed narrowing on increasing T is due to the dynamics of the superparamagnetic behaviour.

4. Discussion

4.1. High-field magnetization

We used a non-interacting-particle model to obtain the best-fit parameters for the magnetic moment of the particles and their anisotropy. We considered particles of volume V, possessing

a magnetic moment $M_s V$, where M_s is the saturation magnetization. In what follows we will assume that the applied magnetic field is along the z-axis. The magnetization direction is specified by the polar and azimuthal angles (θ_M, ϕ_M). The Zeeman energy is given by

$$E_Z = -M_s V H \cos \theta_M. \tag{4.1}$$

Similarly a uniaxial anisotropy axis can be defined by the angles (θ_A, ϕ_A) and this term can be written as

$$E_A = K V \sin^2 \psi \tag{4.2}$$

where ψ is the angle between the anisotropy axis and the magnetization, and

$$\cos \psi = \sin \theta_A \sin \theta_M \cos(\phi_A - \phi_M) + \cos \theta_M \cos \theta_A.$$

The magnetization was then calculated by averaging over randomly distributed easy axes and over a volume distribution given by a log–normal probability density:

$$P(V) = C \exp(-\ln^2(V/V_0)/2\sigma_V^2) \tag{4.3}$$

where $P(V)$ is maximum at V_0, σ_V is the standard deviation of $\ln(V/V_0)$, and C is a normalization constant. We used the modified Langevin function given by Müller and Thursley [23] for the magnetization:

$$M = \frac{M_s}{4\pi} \int_V \int_{\Omega_A} \left[\left(\int_{\Omega_M} \cos \theta_M e^{-E/k_B T} \, d\Omega_M \right) \Big/ \left(\int_{\Omega_M} e^{-E/k_B T} \, d\Omega_M \right) \right] d\Omega_A \, P(V) \, dV \tag{4.4}$$

where $E = E_Z + E_A$, $d\Omega_M = \sin \theta_M \, d\theta_M \, d\phi_M$, and $d\Omega_A = \sin \theta_A \, d\theta_A \, d\phi_A$. The magnetization, calculated using equation (4.4), was introduced into a non-linear least-squares routine to obtain the best-fit parameters. The dotted curves in figure 1 and figure 2 connect the values of $M(H, T)$ calculated using this model. At high H we expect any inter-particle interaction to be overwhelmed by the Zeeman interaction. Therefore only the high-field data ($H > 30$ kOe) were used in the fit which was performed on all of the data obtained at different T, optimizing M_s, K, the average volume, and σ_V simultaneously. From this fit we obtained $M_s = 646 \pm 67$ emu cm^{-3}, $K = 2.0 \pm 1.1 \times 10^7$ erg cm^{-3}, $\langle V \rangle = 117 \pm 41$ Å^3, and $\sigma_V = 0.46 \pm 0.17$. The saturation magnetization is noticeably reduced from the bulk value, $M_s = 1470$ emu cm^{-3}, indicating a possible oxidation, consistent with the susceptibility measurements at higher T (figure 3). The particle volume derived from this fit is extremely small. Considering a FCC structure, with a lattice parameter [22] $a = 3.54$ Å, we can estimate a single-atom volume to be $\sim a^3/4 = 11.1$ Å^3. This would indicate that the magnetic clusters are of only ~ 10 atoms.

The fits to the high-field data for the HT sample are shown in figure 2 by dotted curves. The best-fit values for the parameters were as follows: $M_s = 1700 \pm 285$ emu cm^{-3}, $K = (8.5 \pm 6.7) \times 10^7$ erg cm^{-3}, $\langle V \rangle = 77 \pm 40$ Å^3, and $\sigma_V = 0.74 \pm 0.21$. However, the fitted parameters do not reproduce well the data for low and moderate fields ($H < 20\,000$ Oe), which may be an indication of the effect of inter-particle interactions.

The results for the HT sample indicate that:

(a) The anisotropy is of the same order of magnitude as the values determined for other Co nanoparticles [8, 14], but much larger than the crystalline anisotropy value observed for thin FCC films [22] ($K < 1 \times 10^6$ erg cm^{-3}).

(b) A larger dispersion (σ_V) was found in the HT sample as compared with the AP sample.

(c) The best-fit value of M_s (horizontal dotted curve in figure 2) is larger than that for the bulk, indicating that the heat treatment is effective in reducing the Co to its metallic state.

It is difficult to estimate a shape anisotropy energy without knowing the actual shape of the clusters. For an ensemble of nine atoms arranged as a linear chain, or as a square of 3×3 atoms, the anisotropy energy would be [24] $\approx 0.93\pi M_s^2$ or $\approx 0.98\pi M_s^2$ respectively. The actual cluster shapes are most probably much more compact than a linear or square arrangement, as suggested by experimental [25] and theoretical studies [26], leading to a subsequent reduction of the shape anisotropy energy. An upper limit to the magnetostatic energy could be estimated as half the maximum value calculated above: $(1/2)(0.98\pi M_s^2) \approx 4 \times 10^6$ erg cm^{-3}, which is an order of magnitude smaller than the anisotropy energy derived from the data. From these estimates we conclude that the uniaxial anisotropy cannot be attributed solely to a demagnetizing shape factor and it should be considered as a second-order effect.

The enhancement of M_s relative to the bulk value is in agreement with experimental findings in Co-cluster-beam experiments [5]. This effect was also observed recently [16] for other Co/Ag nanoparticles prepared by the same chemical methods. In that work, however, M_s was found by extrapolating $M(H, T)$ versus $(1/H)$ to $(1/H) \to 0$ at $T = 2$ K without considering the anisotropy effect on the approach to saturation. A large enhancement of M_s (of up to 30%) has also been reported [8] for larger Co colloidal particles (280–4000 atoms). However, atomic beam experiments [5] have shown that $M_s \to M_s$(bulk) for cluster sizes greater than ≈ 400 atoms.

The process of nucleation of larger clusters starts to appear clearly at annealing temperatures $T_A \geqslant 523$ K, as is evident from previous magnetization measurements [16], where two peaks in the ZFC magnetization were observed, one at around 6 K and another broader peak at around 150 K. This irreversible annealing effect was also observed in our sample by means of EPR, as already mentioned. At higher annealing temperatures the χ_{ZFC}-maximum at 6 K decreases in amplitude and the high-T maximum shifts towards higher T and reaches a susceptibility maximum close to room temperature for an annealing temperature of 573 K. Finally, for annealing temperatures of $T_A \geqslant 823$ K, larger (multidomain) particles are formed leading to a reduction in the coercive fields as was reported previously [6].

4.2. Low-field magnetization

The ZFC magnetization data can be interpreted following the theory for single-domain magnetic particles with uniaxial anisotropy. The anisotropy energy gives rise to a two-well potential. The magnetization will relax to its equilibrium following an Arrhenius law given by

$$\tau = \tau_0 \exp(\Delta E / k_B T) \tag{4.5}$$

where $\Delta E = KV$ is the energy barrier under the Stoner–Wohlfarth [27] assumption and $\tau_0 \approx 10^{-11}$ s [17]. Below a certain blocking temperature, T_B, the magnetization will not relax within the measuring time ($\tau_m \approx 100$ s in our case). Under these assumptions, T_B is given by the condition $\tau = \tau_m$ resulting in the relation

$$KV \approx 30 k_B T_B. \tag{4.6}$$

At $T = T_B$, the ZFC magnetization will present a maximum. In real samples the particles are most likely to have a volume distribution. In this case the temperature at which a magnetization maximum occurs, T_m, will be shifted from the T_B associated with the most probable volume [18].

Using the values K, M_s, $\langle V \rangle$, and σ_V obtained from the high-field magnetization data, and assuming a model of non-interacting particles, it is easy to calculate T_m, the temperature at which χ_{ZFC} is maximum. Within this model [18] for a probability density $P(V)$, each particle

of volume V will give a contribution to the susceptibility given by

$$\chi = \begin{cases} 0 & T < T_B \\ (M_s V)^2 P(V)/3k_B & T > T_B. \end{cases} \tag{4.7}$$

Here T_B is the blocking temperature given by equation (4.6). Using this simple model we obtained $T_m(\text{calc}) = 1.5$ K and 3.75 K for the AP and HT samples respectively. These results are consistent with the experimental observations: for the AP sample, $T_m(\text{exp}) < 2.0$ K, while for the HT sample, $T_m(\text{exp}) = 6.0$ K (higher than the calculated T_m). We want to remark that $T_m(\text{calc})$ is close to $T_m(\text{exp})$, which is a further check that the anisotropy and volume determined from the high-field magnetization data are consistent with low-field data. The difference, $T_m(\text{exp}) - T_m(\text{calc})$, found for the HT sample may be due to ferromagnetic inter-particle interactions which have been observed to increase the blocking temperature [17].

Evidence for inter-particle interactions can be deduced from magnetization data at low field ($H < 5000$ Oe), where the anisotropy has negligible effects on $M(H, T)$ [23]. In non-interacting-particle models, $M(H, T)$ should scale with H/T in the absence of interactions. We observed that the HT sample below $T = 30$ K did not follow this scaling law. This is not surprising since at a 10% Co concentration in Ag we can expect interactions between the clusters to be present. Though the study of interactions [28, 29] is of great importance for concentrated magnetic nanoparticles, such a study is beyond the scope of this paper.

4.3. EPR

To analyse the data we used a model initially proposed by de Biasi and Devezas [20], and more recently extended by Berger *et al* [21]. In the case of a strong external magnetic field, the magnetic moment of the particles will be aligned, to a first approximation, parallel to the applied field. In this case the resonance condition (assuming no shape anisotropy) can be approximated by

$$\omega/\gamma = H + H_A(\psi) \tag{4.8}$$

where $\omega = 2\pi\nu$, $\gamma = g\mu_B/\hbar$, H is the applied field, and $H_A(\psi)$ is the anisotropy field given by

$$H_A(\psi) = \frac{K}{M_s}[3\cos^2\psi - 1] \tag{4.9}$$

where ψ is the angle between the magnetization and the anisotropy axis. In the superparamagnetic regime, thermal fluctuations of the magnetic moments result in a dynamic narrowing of the resonance spectra given by [20]

$$H_A^{SP} = H_A(\psi)[1 - 3L(x)/x]/L(x) \tag{4.10}$$

where

$$L(x) = \coth(x) - 1/x$$

is the usual Langevin function, and $x = M_S V H/k_B T$.

The magnetic resonance spectrum of a collection of randomly oriented, non-interacting magnetic particles can be calculated as [21]

$$dI/dH \propto \int_V \int_\psi \mathcal{F} \sin\psi \, d\psi \, V P(V) \, dV \tag{4.11}$$

where $\mathcal{F}$ is the line-shape function which we took as

$$\mathcal{F} \propto u/(1 + u^2)^2$$

with

$$u = [(H + H_A^{SP}) - \omega/\gamma]/\Delta H_i$$

with an intrinsic linewidth ΔH_i. The EPR intensity is proportional to the particle volume, which has been explicitly written in equation (4.11). The volume distribution, $P(V)$, is given by the functional form (4.3). Also K and M_s were taken as independent of V and T.

Within this theory the central part of the EPR (the fit indicated by circles in figure 4) is well reproduced for all T within a consistent set of parameters: the peak-to-peak linewidth, ΔH_{pp}, decreases with T in accordance with the dynamic narrowing expected for superparamagnetic resonance of nanoparticles. The volume dispersion was best fitted to $\sigma_V = 0.3 \pm 0.2$, in agreement with the $M(H, T)$ result. The intrinsic linewidth, ΔH_i, was left free at each T. We found a monotonic decrease of ΔH_i with T (going from 190 ± 30 Oe at 300 K to 90 ± 12 Oe at 500 K), where in all cases $\Delta H_i < \Delta H_{pp}$. Also the centres of the spectra were allowed to vary for each fit, finding an increase of the resonance field with increasing temperature. This feature has also been observed in other experiments on the EPR of magnetic nanoparticles [19, 30].

For the theory outlined above (for the given values of H and T), it turns out that the calculated EPR spectra are sensitive to the anisotropy energy barrier of the particles ($\sim KV$) and not to K and V separately. The energy barrier was found to be approximately constant for all T, yielding $\langle KV \rangle_{EPR} = (6.4 \pm 0.6) \times 10^{-15}$ erg as opposed to the value $\langle KV \rangle_M = (2.0 \pm 1.5) \times 10^{-15}$ erg obtained from $M(H, T)$ at low T. This result confirms that the clusters are indeed small and the anisotropy value is much larger than the bulk value: fixing the anisotropy value to the one obtained from the magnetization data, we get an average cluster size of 30 ± 15 atoms while if we keep the cluster size at the average of 10 atoms, as obtained from $M(H, T)$, we obtain from the EPR spectra $K = (7 \pm 3) \times 10^7$ erg cm^{-3}.

The EPR result for KV is somewhat surprising, since we would have expected the anisotropy constant to decrease with increasing T, leading to KV-values (from EPR at high T) smaller than the ones obtained from $M(H, T)$ at low T. A possible explanation as to the origin of this difference may lie in the fact that the experiments are carried out at two very different characteristic measuring times: 100 s in magnetization measurements and 10^{-9} s in the EPR measurements. This would imply that the characteristic blocking temperature would be at least six times larger in the EPR experiment (considering a characteristic fluctuation time of 10^{-11} s), which would result in a larger effective EPR anisotropy barrier [17].

In figure 6 we show the EPR spectra of the HT sample at three different temperatures. The three spectra shown were fitted (circles) with the same saturation magnetization, the same average volume, and identical log–normal volume distributions ($\sigma_V = 0.74$), as obtained from $M(H, T)$ at low T. The fit qualitatively reproduces well the larger signal 'tails' (as compared with the AP sample; see figure 4) originating in a broader volume distribution, consistent with a larger σ_V obtained from the $M(H, T)$ data. The anisotropy was left as a free parameter in the fit, as were the intrinsic linewidth, the central resonance field, and the amplitude of each scan. The parameters obtained from the fit yield $\langle KV \rangle_{EPR} = (7.3 \pm 4.0) \times 10^{-15}$ erg, as compared with the value $\langle KV \rangle_M = (6.5 \pm 6.0) \times 10^{-15}$ erg obtained from $M(H, T)$ at low T. In this case we can say that the anisotropy energy, as obtained from the EPR, agrees with the value determined from $M(H, T)$. Yet, as mentioned above, we would have expected the anisotropy barrier, as measured by means of EPR at higher values of T, to be smaller than the value obtained from magnetization measurements at lower values of T. We can add that the quality of the EPR spectra taken at $T = 155$ K is poorer than at higher values of T. In the $T = 155$ K spectrum the signal 'tails' extend further than the fit. This may indicate that in low-T EPR, the dynamic averaging due to fluctuations is becoming less effective.

5. Conclusions

Our results show that the microemulsion technique is suitable for preparing clusters of a few atoms with small size dispersion. In the as-prepared sample the magnetization saturates at a value much smaller than for the corresponding bulk Co, indicating a partially oxidized state which is reduced under a mild heat treatment under a flowing H_2 atmosphere at 373 K. After this heat treatment the magnetization extrapolates to values larger than that for the bulk, in accordance with recent experimental results from Co cluster experiments and theoretical predictions. After the heat treatment a wider volume distribution is deduced from the magnetization measurements. EPR is shown to be a very sensitive tool for observing sample transformations, such as the one occurring at 535 K in the AP sample. EPR spectra show line profiles which can be understood as corresponding to dynamically narrowed superparamagnetic resonance. The lines narrow as T increases, following closely the predictions for the EPR of nanoparticles. Both the EPR and magnetization results are consistent as regards the smallness of the clusters, indicating an average of only ≈ 10 atoms per cluster. From the EPR least-squares fits we deduced larger anisotropy barriers than the ones resulting from the magnetization measurements, yet of the same order of magnitude. As far as we know, this is the first work in which the anisotropy energy is determined simultaneously by magnetization and EPR measurements. We believe that combined $M(H, T)$ and EPR results may help us to understand the behaviour of very small clusters in the superparamagnetic regime. The way in which inter-particle interactions modify the low-T magnetization and EPR spectra remains are an open question that requires further analysis.

Acknowledgments

References

[1] Chien C L 1991 *Science and Technology of Nanostructurated Magnetic Materials* ed G C Hadjipanayis and G A Prinz (New York: Plenum)
[2] Reddy R V, Khanna S N and Dunlap B I 1993 *Phys. Rev. Lett.* **70** 3323
[3] Dorantes-Dávila J, Dreyssé H and Pastor G M 1992 *Phys. Rev.* B **46** 10 432
[4] Cox A J, Louderback J G and Bloomfield L A 1993 *Phys. Rev. Lett.* **71** 923
[5] Billas I M L, Châtelain A and de Heer W A 1994 *Science* **265** 1682 and references therein
[6] Rivas J, Sánchez R D, Fondado A, Izco C, García-Bastida A J, García-Otero J, Mira J, Baldomir D, González A, Lado I, López Quintela M A and Oseroff S B 1994 *J. Appl. Phys.* **76** 6564
[7] Becker J A, Schäfer R, Festag F, Ruland W, Wendorff J H, Pebler J, Quasier S A, Helbig W and Reetz M T 1995 *J. Chem. Phys.* **103** 2520
[8] Chen J P, Sorensen C M, Klabunde K J and Hadjipanayis G C 1995 *Phys. Rev.* B **51** 11 527
[9] Leslie-Pelecky D L, Zhang X Q and Rieke R D 1996 *J. Appl. Phys.* **79** 5312
[10] Respaud M, Broto J M, Rakoto H, Fert A R, Thomas L, Barbara B, Verelst M, Snoeck E, Lecante P, Mosset A, Osuna J, Oulk Ely T, Amiens C and Chaudret B 1998 *Phys. Rev.* B **57** 2925
[11] Respaud M, Goiran M, Broto J M, Yang F H, Oulk Ely T, Amiens C and Chaudret B 1999 *Phys. Rev.* B **59** 3934
[12] Gangopadhyay S, Hadjipanayis G C, Sorensen C M and Klabunde K J 1993 *IEEE Trans. Magn.* **29** 2602 Gangopadhyay S, Hadjipanayis G C, Sorensen C M and Klabunde K J 1993 *IEEE Trans. Magn.* **29** 2619
[13] Eastham D A, Qiang Y, Maddock T H, Draft J, Schille J P, Thompson G S and Haberland H 1997 *J. Phys.: Condens. Matter* **9** L497
[14] Slade S B, Parker F T and Berkowitz A E 1994 *J. Appl. Phys.* **75** 6613

[15] Guevara J, Llois A M and Weissmann M 1998 *Phys. Rev. Lett.* **81** 5306

[16] García-Bastida A J, Sánchez R D, Lopez Quintela A M, Rivas J, Ramos C A and Zysler R D 1998 *Non-Crystalline and Nanoscale Materials* ed J Rivas and M A López Quintela (Singapore: World Scientific) pp 475–80

[17] Dormann J L, Fiorani D and Tronc E 1997 *Adv. Chem. Phys.* **98** 283

[18] Wohlfarth E P 1979 *Phys. Lett.* A **70** 489

[19] Nagata K and Ishihara A 1992 *J. Magn. Magn. Mater.* **104–107** 1571

[20] de Biasi R S and Devezas T C 1978 *J. Appl. Phys.* **49** 2466

[21] Berger R, Bissey J-C, Kliava J and Soulard B 1997 *J. Magn. Magn. Mater.* **167** 129

[22] Santos V C, Fernandes A A, Fullerton E E and Ramos C A 1999 *Mater. Sci. Forum* **302+303** 76

[23] Müller K and Thursley F 1973 *Int. J. Magn.* **5** 203

[24] Cullity B D 1972 *Introduction to Magnetic Materials* (New York: Addison-Wesley) p 618

[25] Sakurai M, Watanabe K, Sumiyama D and Suzuki K 1998 *J. Phys. Soc. Japan* **67** 2571 and references therein

[26] Pastor G M, Hirsch R and Mühlschlegel B 1996 *Phys. Rev.* B **53** 10 382 and references therein

[27] Stoner E C and Wohlfarth E P 1948 *Phil. Trans. R. Soc.* A **240** 599

[28] Dormann J L, Cherakaoui R, Sinu L, Nogues M, Lucari F, D'Orazio F, Fiorani D, Tronc E and Jolivet J P 1998 *J. Magn. Magn. Mater.* **187** L139

[29] Kechrakos D and Trohidou K N 1998 *Phys. Rev.* B **58** 12 169

[30] Gazeau F, Bacri J C, Gendron F, Perynski R, Raikher Yu L, Stepanov V I and Dubois E 1998 *J. Magn. Magn. Mater.* **186** 175